The Astrophysical Journal, 854:165 (9pp), 2018 February 20 https://doi.org/10.3847/1538-4357/aaa671
© 2018. The American Astronomical Society. All rights reserved.

Calvera: A Low-mass Strangeon Star Torqued by Debris Disk?

Yunyang Li[1], Weiyang Wang[1,2,3], Mingyu Ge[4], Xiongwei Liu[5], Hao Tong[6], and Renxin Xu[1,7]
[1] School of Physics and State Key Laboratory of Nuclear Physics and Technology, Peking University, Beijing 100871, People's Republic of China; liyunyang@pku.edu.cn
[2] Key Laboratory of Computational Astrophysics, National Astronomical Observatories, CAS, Beijing 100012, People's Republic of China
[3] School of Astronomy and Space Sciences, University of Chinese Academy of Sciences, Beijing 100049, People's Republic of China
[4] Key Laboratory for Particle Astrophysics, Institute of High Energy Physics, Chinese Academy of Sciences, Beijing 100049, People's Republic of China
[5] School of Physics and Space Science, China West Normal University, Nanchong 637002, People's Republic of China
[6] School of Physics and Electronic Engineering, Guangzhou University, Guangzhou 510006, People's Republic of China
[7] Kavli Institute for Astronomy and Astrophysics, Peking University, Beijing 100871, People's Republic of China
Received 2017 September 17; revised 2017 November 26; accepted 2018 January 5; published 2018 February 23

Abstract

Calvera is a unique 59 ms isolated pulsar, because it cannot be detected by radio, optical, and gamma-rays; however, it is detectable through the purely thermal emission in soft X-rays. It is suggested that Calvera could be an ordinary middle-aged pulsar with significant magnetospheric activity at a large distance. Alternatively, it is proposed in this paper that Calvera is a low-mass strangeon star with an inactive magnetosphere (dead). In this scenario, we jointly fit the spectra obtained by the *XMM-Newton* Observatory and the *Chandra* X-ray Observatory with the strangeon star atmosphere model. The spectral model is successful in explaining the radiation properties of Calvera and X-ray dim isolated neutron stars, both of which show similar observation features. Within the dead pulsar picture, Calvera might have a high temperature at 0.67 keV, possess a small stellar radius, $R \lesssim 4$ km, presumably have a small magnetic field, $B \lesssim 10^{11}$ G, and is probably braked by the fallback disk accretion. Future advanced facilities may provide unique opportunities to understand the real nature of Calvera.

Key words: accretion, accretion disks – pulsars: individual (Calvera1RXS J141256.0+792204) – stars: neutron

1. Introduction

The *ROSAT* All-Sky Survey discovered a high galactic latitude ($b = 37°$) compact object, 1RXS J141256.0+792204 (Rutledge et al. 2008), which was then identified as an isolated neutron star (INS; hereafter NS refers to all kinds of pulsar-like compact objects) candidate. The fact that this INS is discovered after the seven radio-quiet and thermally emitting X-ray dim isolated neutron star (XDINS), the Magnificent Seven (see Haberl 2007; Kaplan 2008, for reviews), leads it to be nicknamed "Calvera." Calvera is a puzzling source that has some confusion in its classification among the neutron star family.

Calvera exhibits X-ray pulsations with period $P = 59$ ms and spin-down rate $\dot{P} = 3.2 \times 10^{-15}$ s s^{-1} (Halpern et al. 2013; Halpern & Gotthelf 2015), making its location in the P–$\dot{P}$ diagram (Figure 1) far from the Magnificent Seven, which are slowly rotating ($P \sim 3$–11 s) NSs. It is also speculated that Calvera might be a candidate of the central compact object (CCO; Rutledge et al. 2008; Zane et al. 2011; Gotthelf et al. 2013). However, Calvera presents a larger dipole magnetic field (Shevchuk et al. 2009), and there is still no conclusive evidence for the presence of a host supernova remnant (Zane et al. 2011). Alternatively, there are suggestions that the magnetic field ($\sim 10^{12}$ G) of CCO is buried by prompt fallback of a small amount of supernova ejecta (Ho 2011; Viganò & Pons 2012; Bernal et al. 2013); therefore, Calvera could be a descendant of the CCO re-emerging the magnetic field (Halpern et al. 2013).

It is odd that deep searches failed to detect the radio emission from this source (Hessels et al. 2007; Zane et al. 2011). The non-detection of radio emission from Calvera cannot simply be attributed to the unfavored beaming effect, as emission features are not found in gamma-rays (Halpern 2011; Halpern et al. 2013), which commonly correspond to a larger beaming angle. This can be explained by a distant location of Calvera (e.g., 1.5–5 kpc, Shibanov et al. 2016), but that would place it high above the Galactic disk and cause problem for its birth place. Moreover, attempts also failed in searching for non-thermal emission feature in the soft X-ray band (Zane et al. 2011; Halpern et al. 2013). All of these observational facts could contain hints for the inactive-magnetosphere (i.e., dead) scenario discussed in this work.

The dead-pulsar scenario is hardly understood in the framework of NS, due to its high position above the NS death line (Figure 1). Spectral fits for Calvera with a neutron star atmosphere model result in small emission-radius-to-distance ratio, which forces Shibanov et al. (2016) to conclude a large distance. Alternatively, this problem is avoided if we interpret Calvera as a small-radius strangeon star. Strangeon (Lai & Xu 2017), previously known as strange quark-cluster (Xu 2003), is a prospective candidate for the pulsar constituent and has been successfully applied to solving problems including glitches (Zhou et al. 2014); high mass NS (Lai & Xu 2009, 2011); and ultra low-mass and small-radius NS (Li et al. 2015). It is worth noting that the strangeon star model has passed the examination of tidal polarizability of GW170817 (Abbott et al. 2017; Lai et al. 2017). A radiative model of the strangeon star atmosphere (SSA; Wang et al. 2017a, 2017b) is developed to solve the optical/ultra-violet (UV) excess problem (Walter & Matthews 1997; van Kerkwijk & Kulkarni 2001; Kaplan et al. 2011) and the Rayleigh–Jeans deviation problem (Kaplan et al. 2011) of XDINSs. The luminosity of a strangeon star is maintained by accretion (Wang et al. 2017b), which would also exert a braking torque accounting for the spin-down rate. It is proposed here that Calvera is a low-mass strangeon star with an inactive magnetosphere and probably braked by the accretion flow. In this picture, Calvera and

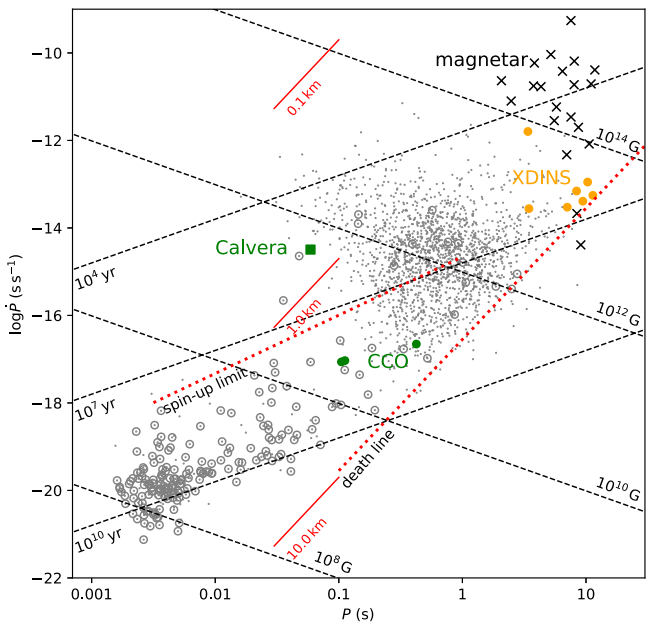

Figure 1. P–$\dot{P}$ diagram for radio pulsars (gray dots), binary pulsars (circlets), magnetars (crosses), XDINSs (orange dots), CCOs (green dots), and Calvera (green square). The pulsar population data are from ATNF Pulsar Catalog (http://www.atnf.csiro.au/research/pulsar/psrcat) (Manchester et al. 2005). The spin data of the three CCOs are from Halpern & Gotthelf (2010) and Gotthelf et al. (2013). The spin-up limit is shown as the upper red dotted line ($P = 1.9(B/10^9\ \mathrm{G})^{6/7}$ ms, van den Heuvel 1987). The death line for a typical $R = 10$ km neutron star is indicated by the lower red dotted line ($\mathrm{BP}^{-2} = 1.7 \times 10^{11}\ \mathrm{G\ s^{-2}}$, Bhattacharya et al. 1992). The death lines for a low-mass strangeon star with two times the nuclear density and different stellar radii are denoted as red solid lines, on the assumption that a pulsar is torqued by magnetospheric activity.

XDINSs, having similar radiative properties, can be understood as strangeon stars at different stages of evolution.

We introduce the data reduction procedure and spectra modeling in Sections 2 and 3, respectively. In Section 4, we constrain the parameters of Calvera as an isolated dead pulsar, while in Section 5 we reconsider this issue by taking into account the accretion effects. We discuss the nature of Calvera in Section 6. A summary and future possible observations in constraining the nature of Calvera are presented in Section 7.

2. Data Reduction

Since the first detection by *ROSAT* (Voges et al. 1999), X-ray observations on Calvera have been made several times by *Swift* (Rutledge et al. 2008), *XMM-Newton* (Zane et al. 2011), and *Chandra* (Shevchuk et al. 2009; Halpern et al. 2013; Halpern & Gotthelf 2015). Despite numerous attempts to model the X-ray spectra, the nature of Calvera still remains open. In this work, we make a joint analysis (also see, Shibanov et al. 2016) of the spectral data obtained by *XMM-Newton* and *Chandra* to further investigate the properties of Calvera. The *Swift* data are omitted due to its limited counting statistics (Rutledge et al. 2008).

2.1. Chandra

We retrieved the *Chandra* Advanced Camera for Imaging and Spectroscopy (ACIS) data from the public archive, among which one (obs. ID 9141; Shevchuk et al. 2009) operated in the VFAINT mode, and two (obs. ID 13788,15613; Halpern et al. 2013) operated in the continuous-clocking (CC) mode. The data reduction and analysis were performed with the *Chandra* Interactive Analysis of Observation (CIAO, version 4.9; Fruscione et al. 2006) with calibration database (CALDB 4.7.4). For obs. ID 9141, we extracted 3599 source photons from a circle centered on the target with radius 4.″16 and 92 background counts from the annulus surrounding the source region with an outer radius of 8.″32. For data obtained in the CC mode, source counts were extracted from a five-column box (15 pixels) centered on the target and the background counts from a five-column box away from the source. The two CC mode observations were weighed by the exposure time and combined together. All *Chandra* spectra were grouped with a minimum of 25 counts per bin. We used the *Chandra* soft band 0.5–2.0 keV for modeling.

2.2. XMM-Newton

The data reduction for *XMM-Newton* were performed with Science Analysis System (SAS, version 16.0.0; SAS development Team 2014). We utilized the European Photon Imaging Camera (EPIC)-pn data of the *XMM-Newton* observations (obs. ID: 0601180101, 0601180201; Zane et al. 2011). Data from the two EPIC-MOS cameras were not used in our analysis due to its smaller effective area at the soft X-ray band (Turner et al. 2001). All observations were obtained in small window (SW) mode with the thin filter. Good time intervals were chosen according to the light curves at 0.1–5 keV band. The source photons were extracted from the circular region with radii 15″ and the background from the adjacent source free region of same size. For spectral analysis, we selected single-pixel events (PATTERN = 0) and excluded bad CCD pixels and columns (FLAG = 0). The *XMM-Newton* spectra were grouped with at least 30 counts per bin; events within the 0.1–3.0 keV range were adopted for modeling.

The information of the data used are summarized in Table 1 for reference. All spectra modeling were performed with XSPEC version 12.9.1 (Arnaud 1996).

3. Spectral Modeling

It is suggested that pulsars could be strangeon stars (see Lai & Xu 2017, for a review). A strangeon star can be thought as a three-flavored gigantic nucleus, and strangeons (coined by combining "strange nucleons") are its constituent as an analogy of nucleons that are the constituent of a normal (micro) nucleus. A strangeon star is self-bounded by residual strong interaction and could therefore have a small mass (e.g., 0.1 $M_\odot$, which could be formed via accretion-induce-collapse of a O-Ne-Mg white dwarf) or a normal mass ($1 \sim 2\ M_\odot$) from massive star core collapse, and reach a mass ceiling of about 3 $M_\odot$ (Guo et al. 2014). The heat capacity of the strangeon matter is very low, so it cools down rapidly after its birth (Yu & Xu 2011; Yuan et al. 2017); therefore, the conventional cooling scenario for thermal X-ray pulsars does not work in the regime of strangeon star. The radiative model of the SSA is put forth by Wang et al. (2017b). For an isolated strangeon star, normal matter (i.e., composed by u, d quarks) accreted onto the stellar surface cannot be converted to strangeons (i.e., strangeonization) instantly, because the collision timescale is far smaller than that of the weak interaction $\tau_{\rm weak} \sim 10^{-7}$ s. Therefore, the unconverted matter would be rebounced and form a thermally emissive atmosphere through bremsstrahlung. As matter is continuously accreted along the magnetic field lines toward the

Table 1
Summary of the X-Ray Data

Data		Instrument/Mode	Counts	Exposure Time (ks)	Start Date	End Date
	9141	ACIS-S(VF)	3599	26.43	2008 Apr 08 03:42:08	2008 Apr 08 12:13:24
Chandra	13788	ACIS-S(CC)	2356	19.68	2013 Feb 12 19:28:07	2013 Feb 13 01:24:58
	15613	ACIS-S(CC)	2155	17.09	2013 Feb 18 02:52:52	2013 Feb 18 08:03:38
XMM-Newton	0601180101	EPIC-pn(SW)	8921	13.94	2009 Aug 31 07:07:52	2009 Aug 31 15:08:42
	0601180201	EPIC-pn(SW)	11411	19.48	2009 Oct 10 04:08:42	2009 Oct 10 12:26:09

Table 2
Summary of Spectral Modeling for Calvera

Model[a]	$N_{\rm H}$ (10^{20} cm^{-2})	kT_e (keV)	y (10^{42} keV km^{-1} cm^{-6})	R^∞ ($d_{\rm kpc}$ km)	E (keV)	τ[b]	EW (eV)	$F_{\rm X}$(0.3–10 keV) 10^{-13} erg cm^{-2} s^{-1}	χ^2_ν/ dof
BB[c]	0	0.2	⋯	0.6	⋯	⋯	⋯	6.2	1.97/482
F	2.7	0.67 ± 0.02	5.6	0.51 ± 0.03	⋯	⋯	⋯	8.4	1.06/482
M1	5.0 ± 0.4	0.64 ± 0.02	0.02	10	⋯	⋯	⋯	10.0	1.04/482
M2	1.3 ± 0.2	0.67 ± 0.02	10.1	0.37	⋯	⋯	⋯	7.7	1.09/482
F	2.7	0.62 ± 0.03	7.6	$0.48^{+0.02}_{-0.01}$	0.72 ± 0.03	0.19 ± 0.02	38^{+27}_{-15}	8.5	1.00/479
M1	5.5 ± 0.4	0.61 ± 0.03	0.02	10	0.73 ± 0.03	0.17 ± 0.02	25^{+14}_{-12}	10.5	1.00/479
M2	1.2 ± 0.2	0.62 ± 0.03	12.5	0.37	0.72 ± 0.02	0.21 ± 0.02	44^{+24}_{-16}	7.7	1.02/479

Notes.
[a] BB: blackbody fit. *F*: $N_{\rm H}$ fixed to the Galactic value; M1: R^∞ fixed to the maximum value to meet the optical upper limit; and M2: R^∞ fixed to the minimum value to meet the blackbody fit.
[b] Optical depth at the absorption line center.
[c] Errors not shown due to poor fit.

polar cap region, whereas the phase transition and radiation happen across the whole stellar surface, a non-uniform density distribution of the atmosphere is then expected (Wang et al. 2017a). This explains the ∼10% pulsed fraction of XDINSs (Haberl 2007) and Calvera (18%, Zane et al. 2011), as well as the slight Rayleigh–Jeans deviation of the XDINS optical spectra (Kaplan et al. 2011). The flux of the SSA emission is described as

$$F_\nu^\infty = B_\nu(1 - e^{-2\tau_\infty(\nu)}), \quad (1)$$

where F_ν is the flux at frequency ν, and B_ν is the blackbody spectrum. $\tau_\infty(\nu)$ is the observed optical depth, with the factor 2 accounting for the surface reflection (Wang et al. 2017a), and can be expressed as

$$\tau_\infty(\nu) = 3.92 \times 10^{-45} \frac{n_{\rm i0}^2 (kT_{\rm i})_{\rm keV}}{(h\nu)^{3.5}_{\rm keV} R_{\rm km}} (1 - e^{-\frac{h\nu}{kT_{\rm e}}}), \quad (2)$$

where $n_{\rm i0}$ is the ion density at bottom, $T_{\rm i}$ and $T_{\rm e}$ are the ion and electron temperatures, respectively, and R is the stellar radius. A strangeon star can support an atmosphere with a large variation in mass, and therefore $n_{\rm i0}$ can only be constrained by observation. Wang et al. (2017b) find a thin atmosphere with $n_{\rm i0} \lesssim 10^{21}$ cm^{-3} for XDINSs. We use the notation $y = n_{\rm i0}^2 (kT_{\rm i})_{\rm keV}/R_{\rm km} \sim 10^{42}$ keV km^{-1} cm^{-6} for these degenerate parameters which is different from the one used in Wang et al. (2017a, 2017b) by $1/R$ (the SSA model with this new definition is now uploaded to XSPEC[8] for public use). At lower energies (i.e., optical/UV bands), the optical depths are high, and the radiation behaves like a blackbody. Whereas for soft X-rays, the typical optical depths are small if the atmosphere is thin and the flux can be approximated by $F_\nu = 2\tau(\nu)B_\nu$, which is lower than a pure blackbody spectrum. Therefore, extrapolating the blackbody spectrum obtained in the X-ray band will meet the optical/UV excess problem (Kaplan et al. 2011). There are two consequences if the optical depth is low at soft X-rays: (1) parameter y is partially degenerate with the normalization $(R_{\rm km}/d_{10\,\rm kpc})^2$ (as is the case for Calvera) and the two cannot be determined simultaneously without the knowledge of the optical/UV data; and (2) because the optical/UV excess is expected from a simple extrapolation of the blackbody spectrum in the X-rays, we can use the extrapolation of the pure blackbody fit for X-rays at optical band as a lower limit for the normalization. On the other hand, the optical upper limit were obtained by *Gemini*-North (g band, Rutledge et al. 2008) and Gran Telescopio Canarias (GTC; g', r' bands, Shibanov et al. 2016), which give the upper limit of the normalization.

The phase-averaged spectral analysis was performed simultaneously for data obtained with different detectors or at different times, allowing only the parameter y to vary independently to account for possible cross-calibration uncertainties. The fit was conducted with a blackbody model (BB) and a SSA model with fixed $N_{\rm H}$ (F, with $N_{\rm H}$ fixed to the Galactic value, Kalberla et al. 2005) or R^∞ (M1, M2). The upper limit of the normalization (M1) was chosen, such that the extrapolated spectrum meet the upper limit at GTC g' band. Theoretically, the SSA model looks exactly like the blackbody model when y goes to infinity. However, a single blackbody model does not give a decent fit, which hints a finite y. For M2, we choose a minimum R^∞, i.e., maximum y, such that XSPEC

[8] https://heasarc.gsfc.nasa.gov/xanadu/xspec/models/ssa.html

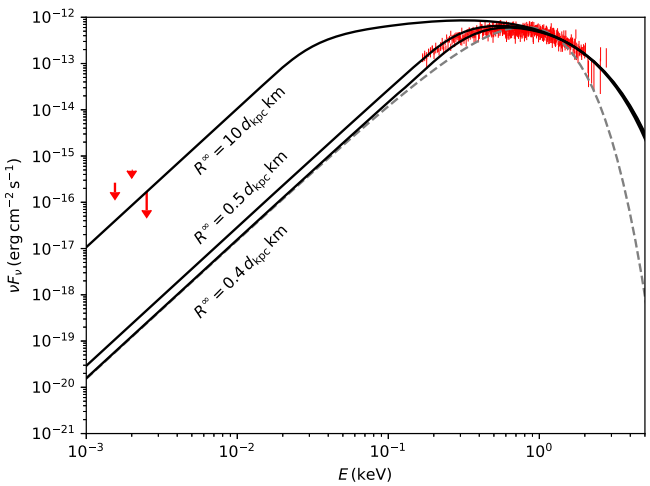

Figure 2. Combined data (red bars) and the fitting results. The red triangle and arrows are the optical flux upper limit given by *Gemini*-North (Rutledge et al. 2008) and GTC (Shibanov et al. 2016). The gray dashed line is the one-component blackbody fitting. The solid lines are the best fits for models F, M1, and M2. Galactic absorption is not shown.

can find a best fit. The results are listed in Table 2 and illustrated in Figure 2.

As is shown in Shevchuk et al. (2009), Zane et al. (2011), and Halpern et al. (2013), single thermal spectra, either blackbody or pure hydrogen atmospheric model (NSA), cannot provide decent fit, and two thermal components are required. The first joint fit for all available data is performed by Shibanov et al. (2016), who use a single-component magnetized hydrogen atmosphere model to account for the inhomogeneities of the stellar surface. Assuming a magnetic field, $B = 10^{12}$ G, they obtain good fits in spite of the viewing geometry. These results are broadly consistent in the sense that $T^\infty \sim 200$ eV for blackbody models and $T^\infty \lesssim 100$ eV for NSA models and emission area $R^\infty/d = 2$–4 km kpc^{-1}(Rutledge et al. 2008; Shevchuk et al. 2009; Zane et al. 2011; Halpern et al. 2013; Shibanov et al. 2016). Zane et al. (2011) report that two thermal models result in $N_{\rm H}$ larger than the Galactic value, while we find that acceptable $N_{\rm H}$ values can be achieved assuming smaller R^∞/d (F and M2). The small stellar value of R^∞/d in the magnetized NSA model lead to the conclusion of a large distance (1.5–5 kpc, Shibanov et al. 2016). As a conservative estimation, a distance as far as 2 kpc places Calvera 1 kpc above the Galactic plane, which is higher than the majority of the pulsar population (Lyne & Graham-Smith 2006). In the strangeon model presented, we have a upper limit of $R^\infty = 10 d_{\rm kpc}$ km, and could have a small stellar radius. It is preferred, though, that the mass of the strangeon star is not so small so that a successful supernova explosion could take place. Adopting a stellar radius of 2 km, corresponding to a few percent of the solar mass, would give a lower estimation of the distance to be ~0.1 kpc. It is worth noting that SSA models (M1, M2, and F) give a higher temperature than that of the BB, and this is also true for XDINSs (Wang et al. 2017b). This deviation (together with the fact that the radiation radius is degenerate with parameter y) indicates that Calvera is also optically thin in X-rays. For an X-ray thin atmosphere, the excess in optical band by a factor of $1/2\tau_{\rm X}$ is often expected, where $\tau_{\rm X}$ is the optical depth at X-rays (e.g., at 1 keV, $1/2\tau_{\rm X} \approx 100/y$). This is only a rough estimation that does not consider the change in the best-fit temperature (e.g., F2 versus BB). The difference in temperature estimation between the SSA and NS model is understandable, as the thermal emission of a strangeon star is from the accretion rather than the residual cooling. Therefore, there is not necessarily a relationship between the pulsar characteristic age and stellar temperature. However, for a certain amount of accretion rate, a smaller stangeon star (i.e., with a smaller reaction area) might build up a higher electron temperature, as is the case for Calvera.

Absorption features at about 0.6–0.7 keV are also reported as lines (Shevchuk et al. 2009; Zane et al. 2011; Shibanov et al. 2016) or edges (Zane et al. 2011). We conducted similar fitting procedure and found that absorption edges or Gaussian absorption lines equally improve the fit for the F, M1, and M2 models. The results for the SSA model multiplied by a `gabs` model are list in Table 2. The additional absorption line is found at 0.73 ± 0.03 keV, which is consistent with Shibanov et al. (2016). The presence of an absorption line is often attributed to the magnetic field. In this case, the absorption line might indicate $B = 6 \times 10^{10}$ G, assuming electron cyclotron of NS.

4. Torqued by Magnetospheric Activity?

In the vacuum gap model for radio emission of neutron stars, Ruderman & Sutherland (1975) propose the idea of a death line, below which the electric potential of the gap region is too low ($<\Phi_c = 10^{12} V$) to generate electron-positron pairs for curvature radiation. The maximum potential drop ($\Phi_{\rm m}$) above the surface of a neutron star is

$$\Phi_{\rm m} = \frac{2\pi^2}{c^2 P^2} {\rm BR}^3, \tag{3}$$

which yields the death line

$$R^3_{\rm max,km} = 1.52 \times 10^2 B_{12}^{-1} P_{\rm s}^2, \tag{4}$$

on the premise that gap sparking could occur if $\Phi_{\rm m} > 10^{12}$ V. Assuming that magnetic dipole radiation accounts for the spin-down, we plot the death lines on the P–$\dot{P}$ diagram (Figure 1) for typical neutron star radius $R = 10$ km (red dotted line) and smaller strangeon star radii (red solid lines). Note that strangeon star with smaller radius (i.e., smaller momentum inertia) would exhibit larger magnetic field than that indicated by the dashed lines in Figure 1. To meet the criterion that Calvera is dead, the upper limit for the stellar radius is 0.66 km, which yields a stellar mass $M = 3 \times 10^{-4}\,M_\odot$. Therefore, in the context of dead pulsar, Calvera can be interpreted as a low-mass strangeon star. However, these values are extreme even for strangeon stars. This problem could be alleviated if alternative mechanisms contribute to the spin-down. In our model (see Section 5), the X-ray emission is maintained by accretion (at a rate $\dot{M}_{\rm X} = 1.2 \times 10^{12} d_{\rm kpc}^2$ g s^{-1} onto the surface), which would also provide a torque braking the rapid-rotating low-mass star and account for the observed $\dot{P}$.

5. Torqued by a Fallback Disk?

The detailed mechanism of the accretion has a significant impact on the long-term evolution, and leads to distinct observational consequences. Two kinds of accretion source are discussed in the literature.

Interstellar medium (ISM) accretion is first proposed by Ostriker et al. (1970) to understand the X-ray luminosity of INS

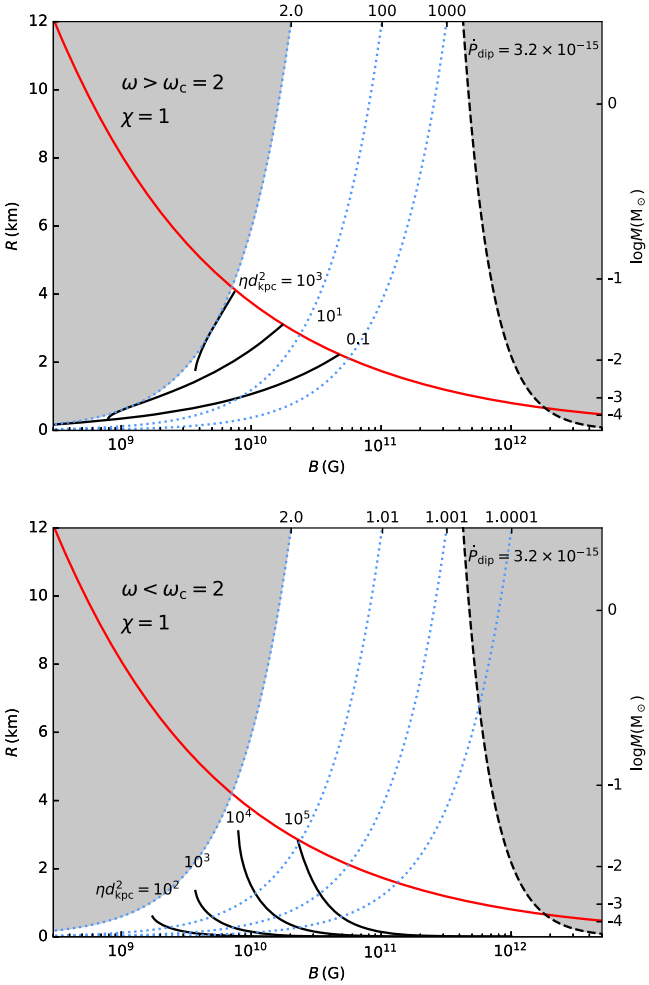

Figure 3. Parameter space of B and R for $\chi = 1$. The upper panel shows the solution to Equation (7), where $\omega > \omega_c(\chi = 1) = 2$, and the lower panel shows $1 \lesssim \omega < \omega_c$. The red solid curve shows the maximum permitted stellar radius of a dead strangeon star. Different choices of $\eta d_{\rm kpc}^2$ are plotted as black solid lines. The black dashed lines are the contours for $\dot{P}_{\rm dip}$, and $\dot{P}_{\rm dip} > 3.2 \times 10^{-15}$ is prohibited. The blue dotted lines are contours for ω with values tag on the top axis and the shaded area on the left corresponds to the area where Equation (7) lacks solution. For most of the permitted parameter space, Calvera experiences a low surface magnetic field.

(Treves & Colpi 1991; Blaes & Madau 1993; also see Treves et al. 2000 for reviews). In this scenario, old INS traveling slowly through dense ISM accrete efficiently and exhibit less luminous ($\lesssim 10^{31}$ erg s^{-1}) thermal soft X-ray spectra. This model may explain the optical excess from the X-ray extrapolation (Zane et al. 2000), which is supported by succeeding observations (e.g., Kaplan et al. 2011).

However, the relatively high proper motion and low ambient ISM density of XDINS cast doubts on the ISM accretion picture. Alternatively, it is reasonable that not all matter are expelled in the supernova explosion (Colgate 1971; Chevalier 1989) and a fractional infalling material may form a fallback disk. The propeller or accretion torques of the disk can explain the high spin-down rate of neutron stars (Alpar 2001; Chatterjee et al. 2000; Ertan et al. 2009, 2014; Benli & Ertan 2016; Ertan et al. 2017), including XDINSs, the anomalous X-ray pulsars and soft gamma-ray repeaters (AXPs and SGRs, see Olausen & Kaspi 2014; Kaspi & Beloborodov 2017, for reviews); the latter are otherwise interpreted as magnetars (Thompson & Duncan 1995). Especially in the picture of Alpar (2001), XDINSs, AXPs, and SGRs which populate a similar region in the P–$\dot{P}$ diagram, can be unified by the asymptotic propeller/accretion mechanism with alternative pathways. In this scenario, the X-ray luminosity of AXP/SGR is caused by accretion (Benli & Ertan 2016), while that of XDINS is produced by energy dissipation in the neutron star (Alpar 2001, 2007) or by intrinsic cooling (Ertan et al. 2014), i.e., accretion onto the stellar surface is not necessarily assumed in the propeller phase. However, matter inflows are observed in simulations of ISM accretion propeller (Romanova et al. 2003), as well as disk accretion propeller (Romanova et al. 2017), and the portion of the accreting matter may be sufficient to maintain the SSA radiation.

Nevertheless, the NS-disk system is not expected to reside in a vacuum. Therefore, we propose here that ISM regulates the debris/fallback disk accretion as a supplement and can be the dominant accretion source in the late phase when the fallback material depletes. In this ISM-fed debris disk accretion (IFDA) picture, we expect $\dot{M}_{\rm A} > \dot{M}_{\rm X} > \dot{M}_{\rm B}$ when the fallback system forms, where $\dot{M}_{\rm B}$ is the ISM accretion rate at the Bondi radius (Bondi 1952), and $\dot{M}_{\rm A}$ is the accretion rate at the Alfvén radius (Ghosh & Lamb 1979). Note that $\dot{M}_{\rm A}$ decreases as the disk loses its mass gradually through accretion and propeller wind. In the late phase of the evolution, the system will reach an equilibrium at $\dot{M}_{\rm X} = \dot{M}_{\rm B} < \dot{M}_{\rm A}$, where the ISM accretion fully accounts for the NS luminosity. At this stage, a disk structure could remain, but it would become thicker as it is fed by the ISM accretion and $\dot{M}_{\rm A}$ does not decrease over time. If the initial mass of the fallback disk is small, the system could also evolve to the spherical ISM accretion regime.

We assume that the fallback disk associated with Calvera is formed. The accreted matter fall in Kaplerian circular orbit toward the Alfvén radius $r_{\rm A}$(Ghosh & Lamb 1979),

$$r_{\rm A} = \left(\frac{B^2R^6}{\dot{M}_{\rm A}\sqrt{2GM}}\right)^{2/7} = 6.18 \times 10^8 B_{12}^{4/7} R_{\rm km}^{12/7} M_{\rm l}^{-1/7} \dot{M}_{\rm A,10}^{-2/7}\ {\rm cm}, \quad (5)$$

where B_{12} is the surface magnetic field in units of 10^{12} G, $R_{\rm km}$ the stellar radius in units of km, $M_{\rm l}$ the stellar mass in units of $M_\odot$, and $\dot{M}_{\rm A,10}$ is the accretion rate at $r_{\rm A}$ in units of 10^{10} g s^{-1}. Matter accumulated at $r_{\rm A}$ will be forced to co-rotate with the NS, and most of the mass would be expelled centrifugally due to the propeller effect (Illarionov & Sunyaev 1975). Consequently, the co-rotation and deflection of the matter would exert a negative torque N on the star which contributes to the spin-down of the pulsar (Liu et al. 2014),

$$N = 2\dot{M}_{\rm A} r_{\rm A}^2 \Omega_{\rm K}(r_{\rm A})\left[1 - \left(\frac{\Omega}{\Omega_{\rm K}(r_{\rm A})}\right)^{\chi}\right] = -I\frac{2\pi}{P^2}\dot{P}, \quad (6)$$

where $\Omega_{\rm K}(r_{\rm A}) = (GM/r_{\rm A}^3)^{1/2}$ is the Keplerian angular velocity at $r_{\rm A}$. The factor χ is introduced to account for the the inefficiency of the propeller effect ($0 < \chi < 1$). This formula reduces to the prevailing form when $\chi = 1$ (Menou et al. 1999; Chatterjee et al. 2000). We assume the momentum inertia of the star to be $I = MR^2/2$, and the mass–radius relation for a low-mass strangeon star can be approximated by $M = 4\pi\rho R^3/3$,

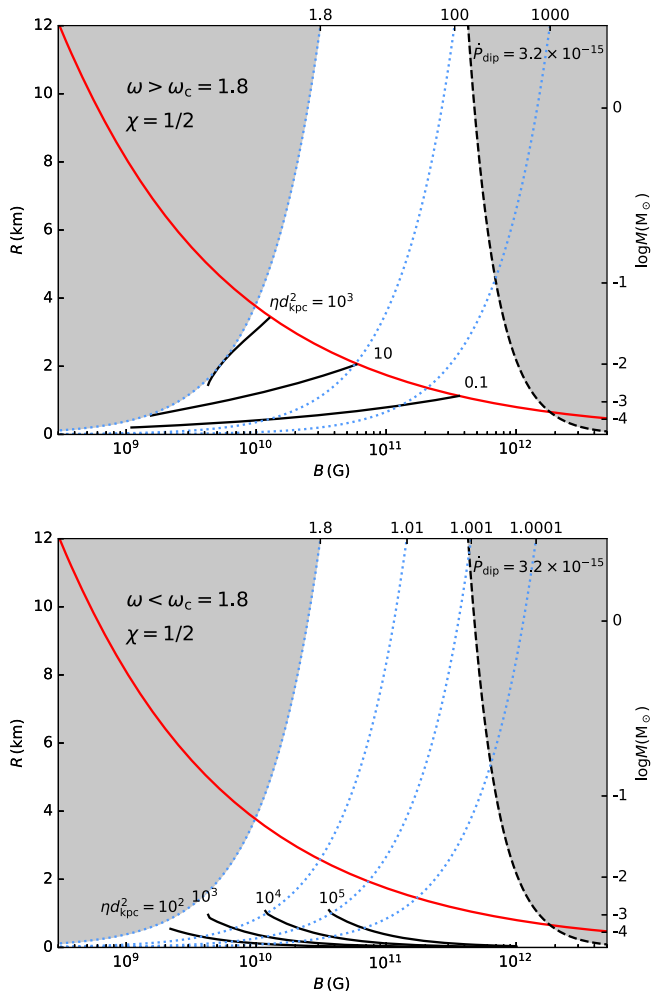

Figure 4. Same as Figure 3, but for $\chi = 1/2$ and $\omega_c(\chi = 1/2) = 1.8$.

where the density ρ is a few times the nuclear density ρ_n (Lai & Xu 2009; Lai et al. 2013; Guo et al. 2014). We fix $\rho = 2\rho_n$. Combining Equations (5) and (6), we obtain

$$\dot{P} = 4.3 \times 10^{-12} B_{12}^{8/7} R_{\rm km}^{-17/7} P_s \dot{M}_{A,10}^{3/7} \frac{\omega^\chi - 1}{\omega} \text{ s s}^{-1}, \quad (7)$$

where the fastness $\omega = \Omega/\Omega_K(r_A)$ and $\omega > 1$ is required in the propeller phase. Substituting $\dot{M}_A$ into ω, we see the bimodality of Equation (7), i.e., solutions with $\omega > \omega_c$ or $1 < \omega < \omega_c$, where $\omega_c = (2/(2-\chi))^{1/\chi}$.

Most of the mass accreted to the the Alfvén radius is expelled, and only a small portion of the matter is accumulated onto the strangeon star surface (Romanova et al. 2017), i.e., $\dot{M}_A = \eta \dot{M}_X$ with $\eta > 1$. $\dot{M}_X$ can be inferred from the X-ray luminosity, $L_X = 4\pi d^2 F_X \approx 0.1 \dot{M}_X c^2$. We use the flux obtained by the spectral fit $F_{X,0.3-10\,\rm keV} = 9.0 \times 10^{-13}$ erg cm^{-2} s^{-1} for calculation. The factor 0.1 is the approximate energy conversion efficiency which is dominated by the gravitational potential for massive star and by the strangeonization energy release for low-mass star.

We present the parameter space of B and R for $\omega > \omega_c$ and $\omega < \omega_c$ in Figures 3 and 4. The red curve is the death-line criterion provided by Equation (4). Contours for $\eta d_{\rm kpc}^2$ are in solid black lines. The black dashed line is the contour for $\dot{P}_{\rm dip}$, and the shaded area on the right is prohibited. The blue dotted lines are the ω contour, and the shaded area on the left is also banned, as there is no solution to Equation (7). The intersection point of the $\omega = \omega_c$ curve and the red curve provides the upper limit of Calvera ($R \lesssim 4$ km, $M \lesssim 0.1\,M_\odot$, regardless of χ), which yields a negligible redshift factor $(1\text{–}2GM/c^2R)^{-1/2} \lesssim 1.1$. For $\omega > \omega_c$, as $\eta > 1$ and the speculation that Calvera can be as close as ~0.3 kpc (Halpern & Gotthelf 2015), $\eta d_{\rm kpc}^2 = 0.1$ can be regarded as a lower limit which yields $B \lesssim 10^{11}$ G. In the $\omega < \omega_c$ case, $\eta d_{\rm kpc}^2$ are so large that the luminosity of Calvera would approach its Eddington limit, moreover, a large $\eta \sim 10^4$ is not favored by simulation (Romanova et al. 2003, 2017). Besides, $\omega < \omega_c$ restricts the fastness in a small region very close to unity, which is not dynamically stable for a fast-rotating young pulsar. We therefore claim that $\omega < \omega_c$ is not likely the case for Calvera. Most of the parameter space agrees with a low magnetic field $B < 10^{11}$ G. The matter accreted to the polar cap diffuse across the star surface with a timescale $\tau \propto B^2$. For Calvera with a small magnetic field, we assume that the radiation is from the entire surface, i.e., $R = R^\infty$, though there is uniformity in the density of the atmosphere. Figures 3 and 4 also show why a neutron star model cannot fit in this propeller scenario. For a typical $R = 10$ km NS, the death-line criterion would require a small magnetic field of 10^8 in the shaded area where there is no possibility to be consistent with the propeller torque (Equation (7)). Although a neutron star does not follow the M$\propto R^3$ equation of state, it has approximately the same average density as a strangeon star. Thus, the argument above is valid.

Jointing the parameters constrained by spectral modeling and the dead-pulsar criterion, in Figure 5 we plot the contours with respect to the stellar (radiation) radius R^∞ and the distance d in the $\omega > \omega_c$ case for $\chi = 1$ and $\chi = 1/2$. The upper and lower limits of the spectral normalization are plotted as black solid lines. The colorful lines within the permitted space represent different combinations of η and B and color coded by B. The contour lines are cut off at the maximum radii (dashed lines), with regard to the value of B. The maximum radius is defined by both the death-line criterion and the fastness criterion; therefore, a lower magnetic field might correspond to a smaller maximum radius (see Figures 3 and 4). The logarithm of η is tagged below each contour line. In both panels, the contours of η begin at larger radii for larger B, i.e., a smaller maximum radius. Therefore, beyond a certain value of $B = 10^{11}$ G, no reasonable η can satisfy the upper limit in optical bands. We conclude that $B \lesssim 10^{11}$ G.

The accretion rate of Calvera responsible for the luminosity is $\dot{M}_X = 1.2 \times 10^{12}\, d_{\rm kpc}^2$ g s^{-1}. For ISM accretion, the accretion rate at the Bondi radius (Bondi 1952) is

$$\dot{M}_B = 4\pi\rho_\infty \frac{(GM)^2}{v^3}, \quad (8)$$

where ρ_∞ is the ISM density, assumed to be $10^{-24}\rho_{24}$ g cm^{-3}, and v the speed of the star which is inferred from the proper motion measurement to be $v_\perp = 286 \pm 110\, d_{\rm kpc}$ km s^{-1} (Halpern & Gotthelf 2015). This results in $\dot{M}_B = 10^7\, \rho_{24} M_1^2 d_{\rm kpc}^{-3}$ g s^{-1} and

$$\frac{\dot{M}_X}{\dot{M}_B} = 10^5 \rho_{24}^{-1} M_1^{-2} d_{\rm kpc}^5. \quad (9)$$

Even for a very small d (e.g., 0.1 kpc), the matter accretes on the stellar surface faster than the Bondi accretion, and $\dot{M}_A = \eta \dot{M}_X \approx 10^{11-15}$ g s^{-1} is even higher. The latter rate is

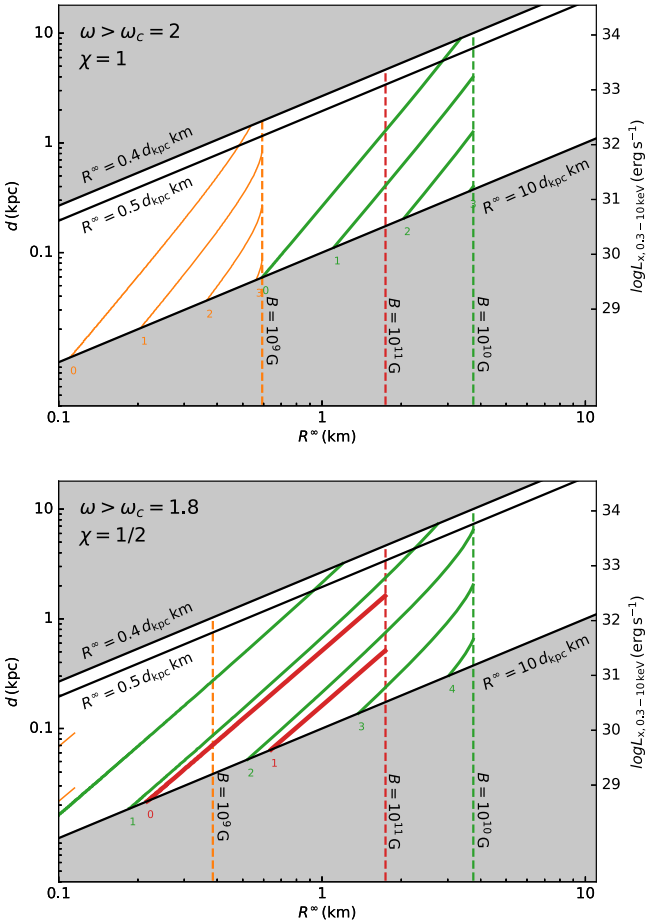

Figure 5. Parameter space of radiation radius (R^∞) and distance (d) for $\omega > \omega_c$, $\chi = 1$ (upper panel) and $\chi = 1/2$ (lower panel). Due to the low redshift factor and the low surface magnetic field, we assume $R^\infty = R$. R^∞/d from models F, M1, and M2 are shown as black solid contour lines. The shaded spaces are prohibited. The colored lines represent different combinations of B and η. Lines are color coded (also with different line thickness) by B, and the contours are cut off at the maximum radii (dashed lines) corresponding to B. The value of η ranges from 1–10^4 and their logarithms are tagged below each line. We regard $\eta = 1$ as a lower bound; consequently, B $\gtrsim 10^{11}$ is unlikely, as the parameter space is limited. We note that these contour lines overlap with each other due to the degeneracy between η and B.

typical for a fallback disk of 10^5 years (Alpar et al. 2001; Ertan et al. 2009), indicating that Calvera is at the early phase of the IFDA evolution, which is often expected from a pulsar with small period.

We illustrate the evolution of Calvera in Figure 6, assuming some choices of χ, R, and B. The decrease of the accretion rate of the fallback disk is modeled by a power law (Menou et al. 2001) $\dot{M}_A = \dot{M}_0(t/T)^{-\alpha}$ (red lines). We set $T = 1000$ s and the current age of Calvera to be the characteristic age 3.2×10^5 years, but the detailed values are not very important. $\alpha = 7/6$ is adopted from Liu et al. (2014), which is similar to that in Cannizzo et al. (1990).

Though not likely to be the accretion source of Calvera, we note that the ISM accretion predicts a braking index $n = \ddot{\Omega}\Omega/\dot{\Omega}^2 \approx \chi$ (assuming that the ISM feed the disk at a constant rate). The fallback disk model, on the other hand, predicts a large braking index in the early evolution (this is of high uncertainty because the self-similar model for the disk might be invalid during the early time) that falls to a value $\sim$1

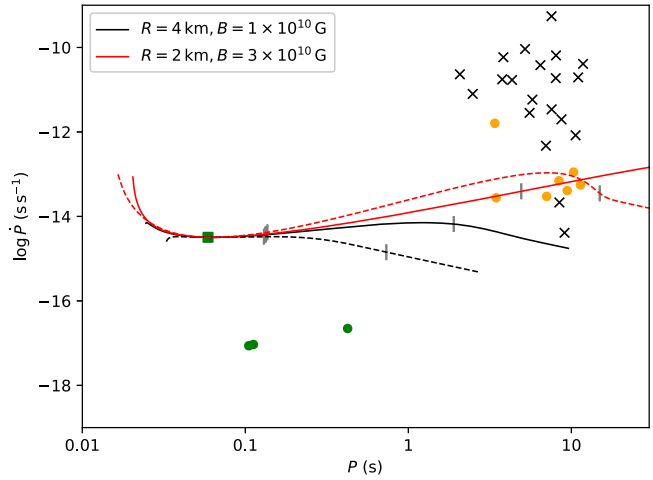

Figure 6. Evolution tracks of Calvera with a fallback disk, assuming $\chi = 1$ (solid curve) and $\chi = 1/2$ (dashed curve). The gray bars anchored on the curves mark the age of 10^6 year and 10^7 year. Pulsar notations are same with those in Figure 1. We use $\dot{M}_A = \dot{M}_0(t/T)^{-\alpha}$, where the timescale $T = 1000$ s, $\alpha = 7/6$ and $\dot{M}_0 \sim 10^{21-25}$ g s^{-1}.

during the migration. It also shows that Calvera would eventually evolve to the XDINS region within $\sim 10^7$ years, and populates in a clustered area. Therefore, Calvera could be a progenitor of XDINS that is self-consistent, as the radiation properties of the latter is also interpreted in the framework of the SSA model (Wang et al. 2017b). In this late phase, transition from the fallback disk accretion to ISM accretion may occur (Wang et al. 2017a).

6. Discussion

6.1. Distance

The distance of Calvera is highly uncertain, due to the lack of radio observation and optical counterpart identification. Generally, the distance estimation can be obtained through three methods: (1) luminosity, (2) N_H column, and (3) proper motion measurement. Unfortunately, the first two methods are spectral-model dependent and the luminosity is even less constrained in the SSA model due to the lack of optical data. For the lower limit of R^∞ in the *XMM-Newton* spectrum fit, we have a lower limit of $N_H = (1.3 \pm 0.2) \times 10^{20}$ cm^{-2}. This value is comparable to the galactic value 2.65×10^{20} cm^{-2} (Kalberla et al. 2005), placing Calvera beyond the radius of the Local Bubble (Cox & Reynolds 1987). For a conservative estimation, we suggest $d > 100$ pc (Lallement et al. 2003; Halpern & Gotthelf 2015) as the distance lower limit.

The model-independent estimation comes from the proper motion measurement. Halpern & Gotthelf (2015) obtain the proper motion of Calvera to be 69 ± 26 mas yr^{-1}, corresponding to a transverse velocity $v_\perp = 286 \pm 110\, d_{kpc}$ km s^{-1} with respect to the local standard of rest. Given the typical transverse velocity of XDINS to be 150–300 km s^{-1} (e.g., Kaplan 2008) and its high galactic latitude, it is not likely that Calvera is a far away pulsar, and $d \lesssim 1$ kpc can be a hypothetical upper limit.

6.2. Calvera as a CCO

The connections between Calvera and the CCO have been hotly debated since its discovery. The non-detection of the supernova remnant (within 2°, Rutledge et al. 2008) places

Calvera as a candidate of the first orphaned CCO. In this work, we provide more evidence for this argument.

The best-fit temperature of Calvera in the context of a neutron star atmosphere result in $\lesssim$0.2 keV (Zane et al. 2011; Shibanov et al. 2016), smaller than that of known CCOs, which are within the range 0.3–0.7 keV (e.g., Pavlov et al. 2001, 2000; Hui & Becker 2006; Park et al. 2006, also see Figure 2 in Rutledge et al. 2008). This was then attributed to the intrinsic cooling; however, the temperature of Calvera in the SSA model $\approx$0.6 keV readily fits in the CCO population.

The main counter argument for Calvera being a CCO is its upper position in the P–$\dot{P}$ diagram (i.e., the high magnetic field). Ho (2011) proposes that the magnetic field can be buried by prompt fallback supernova ejecta and be recovered within 10^4 years. In our accretion-braked dead strangeon star scenario, the magnetic field of Calvera is constrained at $B \lesssim 10^{11}$ G, which brings Calvera closer to the CCO family. In either picture, Calvera can be interpreted as a (orphaned) CCO. A discriminative probe would be the future measurement of the braking index. For an accretion-braked pulsar, $n > 0$ in the early phase, whereas CCO with rapid field growth would exhibit a large negative braking index (Viganò & Pons 2012; Bernal et al. 2013). Unifying CCO and XDINS within the IFDA picture will be presented in an upcoming paper.

7. Summary

In the framework of the strangeon star model, we find a consistent and successful interpretation of Calvera as a dead low-mass strangeon star ($\lesssim 0.1\,M_\odot$) with a small radius ($\lesssim$4 km) and a presumably weak magnetic field ($\lesssim 10^{11}$ G) that is most likely braked by the fallback disk accretion.

Nevertheless, a decisive judgment on the nature of Calvera will only come from future observations. The optical flux measurement will be crucial in determining the $d - R^\infty$ relation (Figure 5). In our optical/UV excess picture, we predict the lower limit of the optical magnitude to be $g' \lesssim$ 35 mag, which is challenging even for future instruments (e.g., Thirty Meter Telescope, Nelson & Sanders 2008). However, it is possible that the optical flux is higher than the lower limit by a factor of 5–12 if the atmosphere is very thin (Kaplan et al. 2011), making it more accessible. Future timing analysis can distinguish the braking mechanisms (either by accretion or by magnetic dipole radiation or by rapid magnetic field growth). The long-term timing monitoring can be achieved with the enhanced X-ray Timing and Polarimetry (eXTP, Zhang et al. 2016); the Neutron star Interior Composition ExploreR (NICER; Gendreau et al. 2012). If Calvera is indeed a near pulsar, a distance measurement will also benefit from the future deep optical observation or soft X-ray timing. Although not possible at present (Zane et al. 2011), future detection of radio and gamma-ray emission will differentiate whether Calvera is a dead pulsar.

We thank Dr. Andrey Danilenko for drawing our attention to this interesting object, Calvera, during his visit to KIAA. We are grateful to all of the members in the pulsar group at Peking University and Dr. Xiangdong Li at Nanjing University for discussions. This work is supported by the National Key R&D Program of China (No. 2017YFA0402600), the National Natural Science Foundation of China (No. 11673002, U1531243, and U1531137), and the Strategic Priority Research Program of CAS (No. XDB23010200).

Software: XSPEC (Arnaud 1996), CIAO (Fruscione et al. 2006), SAS (SAS development Team 2014).

ORCID iDs

Yunyang Li https://orcid.org/0000-0002-4820-1122
Weiyang Wang https://orcid.org/0000-0001-9036-8543
Hao Tong https://orcid.org/0000-0001-7120-4076

References

Abbott, B. P., Abbott, R., Abbott, T. D., et al. 2017, PhRvL, 119, 161101
Alpar, M. A. 2001, ApJ, 554, 1245
Alpar, M. A. 2007, Ap&SS, 308, 133
Alpar, M. A., Ankay, A., & Yazgan, E. 2001, ApJL, 557, L61
Arnaud, K. A. 1996, in ASP conf. Ser. 101, Astronomical Data Analysis Software and Systems, ed. G. H. Jacoby & J. Barnes (San Francisco, CA: ASP), 17
Barret, D., Lam Trong, T., den Herder, J.-W., et al. 2016, Proc. SPIE, 9905, 99052F
Benli, O., & Ertan, Ü. 2016, MNRAS, 457, 4114
Bernal, C. G., Page, D., & Lee, W. H. 2013, ApJ, 770, 106
Bhattacharya, D., Wijers, R. A. M. J., Hartman, J. W., & Verbunt, F. 1992, A&A, 254, 198
Blaes, O., & Madau, P. 1993, ApJ, 403, 690
Bondi, H. 1952, MNRAS, 112, 195
Cannizzo, J. K., Lee, H. M., & Goodman, J. 1990, ApJ, 351, 38
Chatterjee, P., Hernquist, L., & Narayan, R. 2000, ApJ, 534, 373
Chevalier, R. A. 1989, ApJ, 346, 847
Colgate, S. A. 1971, ApJ, 163, 221
Cox, D. P., & Reynolds, R. J. 1987, ARA&A, 25, 303
Ertan, Ü, ćalışkan, Ş, & Alpar, M. A. 2017, MNRAS, 470, 1253
Ertan, Ü, Çalışkan, Ş, Benli, O., & Alpar, M. A. 2014, MNRAS, 444, 1559
Ertan, Ü, Ekşi, K. Y., Erkut, M. H., & Alpar, M. A. 2009, ApJ, 702, 1309
Fruscione, A., McDowell, J. C., Allen, G. E., et al. 2006, Proc. SPIE, 6270, 62701V
Gaskin, J. A., Weisskopf, M. C., Vikhlinin, A., et al. 2015, Proc. SPIE, 9601, 96010J
Gendreau, K. C., Arzoumanian, Z., & Okajima, T. 2012, Proc. SPIE, 8443, 844313
Ghosh, P., & Lamb, F. K. 1979, ApJ, 234, 296
Gotthelf, E. V., Halpern, J. P., & Alford, J. 2013, ApJ, 765, 58
Guo, Y., Lai, X., & Xu, R. 2014, ChPhC, 38, 055101
Haberl, F. 2007, Ap&SS, 308, 181
Halpern, J. P. 2011, ApJL, 736, L3
Halpern, J. P., Bogdanov, S., & Gotthelf, E. V. 2013, ApJ, 778, 120
Halpern, J. P., & Gotthelf, E. V. 2010, ApJ, 709, 436
Halpern, J. P., & Gotthelf, E. V. 2015, ApJ, 812, 61
Hessels, J. W. T., Stappers, B. W., Rutledge, R. E., Fox, D. B., & Shevchuk, A. H. 2007, A&A, 476, 331
Ho, W. C. G. 2011, MNRAS, 414, 2567
Hui, C. Y., & Becker, W. 2006, A&A, 454, 543
Illarionov, A. F., & Sunyaev, R. A. 1975, A&A, 39, 185
Kalberla, P. M. W., Burton, W. B., Hartmann, D., et al. 2005, A&A, 440, 775
Kaplan, D. L. 2008, in AIP Conf. Ser. 983, 40 Years of Pulsars: Millisecond Pulsars, Magnetars and More, ed. C. Bassa et al. (Melville, NY: AIP), 331
Kaplan, D. L., Kamble, A., van Kerkwijk, M. H., & Ho, W. C. G. 2011, ApJ, 736, 117
Kaspi, V. M., & Beloborodov, A. M. 2017, ARA&A, 55, 261
Lai, X. Y., Gao, C. Y., & Xu, R. X. 2013, MNRAS, 431, 3282
Lai, X. Y., & Xu, R. X. 2009, MNRAS, 398, L31
Lai, X.-Y., & Xu, R.-X. 2011, RAA, 11, 687
Lai, X.-Y., & Xu, R.-X. 2017, J. Phys. Conf. Ser., 861, 012027
Lai, X. Y., Yu, Y. W., Zhou, E. P., Li, Y. Y., & Xu, R. X. 2017, RAA, in press (arXiv:1710.04964)
Lallement, R., Welsh, B. Y., Vergely, J. L., Crifo, F., & Sfeir, D. 2003, A&A, 411, 447
Li, Z., Qu, Z., Chen, L., et al. 2015, ApJ, 798, 56
Liu, X.-W., Xu, R.-X., Qiao, G.-J., Han, J.-L., & Tong, H. 2014, RAA, 14, 85
Lyne, A. G., & Graham-Smith, F. 2006, Pulsar Astronomy (Cambridge: Cambridge Univ. Press)
Manchester, R. N., Hobbs, G. B., Teoh, A., & Hobbs, M. 2005, AJ, 129, 1993
Menou, K., Esin, A. A., Narayan, R., et al. 1999, ApJ, 520, 276
Menou, K., Perna, R., & Hernquist, L. 2001, ApJL, 554, L63

Nelson, J., & Sanders, G. H. 2008, Proc. SPIE, 7012, 70121A
Olausen, S. A., & Kaspi, V. M. 2014, ApJS, 212, 6
Ostriker, J. P., Rees, M. J., & Silk, J. 1970, ApL, 6, 179
Park, S., Mori, K., Kargaltsev, O., et al. 2006, ApJL, 653, L37
Pavlov, G. G., Sanwal, D., Kızıltan, B., & Garmire, G. P. 2001, ApJL, 559, L131
Pavlov, G. G., Zavlin, V. E., Aschenbach, B., Trümper, J., & Sanwal, D. 2000, ApJL, 531, L53
Romanova, M. M., Blinova, A. A., Ustyugova, G. V., Koldoba, A. V., & Lovelace, R. V. E. 2017, arXiv:1704.08336
Romanova, M. M., Toropina, O. D., Toropin, Y. M., & Lovelace, R. V. E. 2003, ApJ, 588, 400
Ruderman, M. A., & Sutherland, P. G. 1975, ApJ, 196, 51
Rutledge, R. E., Fox, D. B., & Shevchuk, A. H. 2008, ApJ, 672, 1137
SAS development Team 2014, SAS: Science Analysis System for XMM-Newton observatory, Astrophysics Source Code Library, ascl:1404.004
Shevchuk, A. S. H., Fox, D. B., & Rutledge, R. E. 2009, ApJ, 705, 391
Shibanov, Y., Danilenko, A., Zharikov, S., Shternin, P., & Zyuzin, D. 2016, ApJ, 831, 112
Thompson, C., & Duncan, R. C. 1995, MNRAS, 275, 255
Treves, A., & Colpi, M. 1991, A&A, 241, 107
Treves, A., Turolla, R., Zane, S., & Colpi, M. 2000, PASP, 112, 297
Turner, M. J. L., Abbey, A., Arnaud, M., et al. 2001, A&A, 365, L27
van den Heuvel, E. P. J. 1987, in IAU Symp. 125, The Origin and Evolution of Neutron Stars, ed. D. J. Helfand & J.-H. Huang (Cambridge: Cambridge Univ. Press), 393
van Kerkwijk, M. H., & Kulkarni, S. R. 2001, A&A, 378, 986
Viganò, D., & Pons, J. A. 2012, MNRAS, 425, 2487
Voges, W., Aschenbach, B., Boller, T., et al. 1999, A&A, 349, 389
Walter, F. M., & Matthews, L. D. 1997, Natur, 389, 358
Wang, W., Feng, Y., Lai, X., et al. 2017a, MNRAS, submitted (arXiv:1705.03763)
Wang, W., Lu, J., Tong, H., et al. 2017b, ApJ, 837, 81
Xu, R. X. 2003, ApJL, 596, L59
Yu, M., & Xu, R. X. 2011, APh, 34, 493
Yuan, M., Lu, J.-G., Yang, Z.-L., Lai, X.-Y., & Xu, R.-X. 2017, RAA, 17, 092
Zane, S., Haberl, F., Israel, G. L., et al. 2011, MNRAS, 410, 2428
Zane, S., Turolla, R., & Treves, A. 2000, ApJ, 537, 387
Zhang, S. N., Feroci, M., Santangelo, A., et al. 2016, Proc. SPIE, 9905, 99051Q
Zhou, E. P., Lu, J. G., Tong, H., & Xu, R. X. 2014, MNRAS, 443, 2705